S01. Force Balance in Saturn's Warped Magnetodisc

Nicholas Achilleos[1], C. S. Arridge[2] and P. Guio[1]

[1]Department of Physics and Astronomy, [2]Mullard Space Science Laboratory (both part of the Centre for Planetary Sciences), University College London, UK
Contact: nick@apl.ucl.ac.uk / csa@mssl.ucl.ac.uk / p.guio@ucl.ac.uk
Download Poster: http://www.homepages.ucl.ac.uk/~ucapnac/posters/nach_mop_2009.pdf

July 27-31, 2009

Abstract

In the Cassini era, the north magnetic axis of Saturn's planetary dipole field has been oriented at angles of $> 65^\circ$ with respect to the upstream solar wind flow. This deviation from perfect orthogonality is responsible for the formation of a 'bowl-shaped' current sheet in the outer magnetosphere [3]. In order to investigate the force balance in such a structure, we have started by using the formalism of [5] to construct planar disc structures in which centrifugal, pressure and magnetic ($\boldsymbol{J} \times \boldsymbol{B}$) forces are in equilibrium.

We extend this planar model to produce bowl-shaped geometries through the representation of the magnetopause 'shielding field' with an external dipole, displaced from the planet along the axis of azimuthal symmetry of the modelled system. The location and strength of the external dipole relative to the planetary source determines a curl-free field with north-south asymmetry which, when added to the planetary and disc fields, produces a distortion of the planar disc, 'sweeping' it back from the equatorial plane. We examine the effect on the sheet geometry of the external dipole parameters, and make preliminary comparisons with Cassini magnetometer data.

Introduction

- The planets Jupiter and Saturn have magnetospheres which differ from that of the Earth in many respects. For example, both of these planets have strong internal plasma sources which 'feed' the rapidly rotating discs of plasma situated near the rotational equator. These sources are, for Saturn, the icy moon Enceladus with mass loading rate $\sim 10\,\mathrm{kg\ s^{-1}}$ of water group ions; and, for Jupiter, the moon Io which adds $\sim 500\,\mathrm{kg\ s^{-1}}$ of suphur / oxygen ions. In order to provide the centripetal force required to maintain the rotation of the plasma disc, the magnetic field in the magnetosphere beyond a certain characteristic distance $\mathrm{R_M}$ is radially 'stretched' near the equatorial plane.
- This so-called *magnetodisc* geometry provides an inwards magnetic curvature force which, in a corotating frame of reference, balances the sum of the outward forces due to centrifugal force, plasma pressure gradient and magnetic pressure gradient. [5] showed that, for an azimuthal symmetry, such a field structure has an Euler potential α which is a solution of the differential equation:

$$\frac{\partial^2 \alpha}{\partial r^2} + \frac{1-\mu^2}{r^2}\frac{\partial^2 \alpha}{\partial \mu^2} = -g(r,\mu,\alpha), \tag{1}$$

  where r is radial distance from planet centre (in units of planetary radii); μ is the cosine of colatitude i.e. $\mu = \cos\theta$; and the unit of α used here is $B_0 a$, the product of planetary equatorial magnetic field and planetary radius. The 'source function' g is determined by the global distribution of plasma pressure and angular velocity. Equatorial plasma properties are the 'boundary conditions' which are used to infer global structure, via force balance.

Model Inputs

We use the Cassini observations by [11] (thermal plasma), [9] (hot plasma) and [8] (plasma angular velocity) in order to constrain the model's equatorial plasma properties. To incorporate the response of 'frozen-in' plasma to change in R_{MP}, we specify the profile of flux tube content for the cold plasma (number of ions in a tube of cross-section equal to unit magnetic flux, whose volume varies with the magnetopause radius R_{MP}). We also specify hot plasma pressure beyond $8\,R_S$ by requiring that the product of hot pressure and flux tube volume equal a constant K_h, here equal to 2×10^6 Pa m T^{-1} (although it may vary considerably as the observations show (see Figures)).

Figure 1: Magnetic Potentials

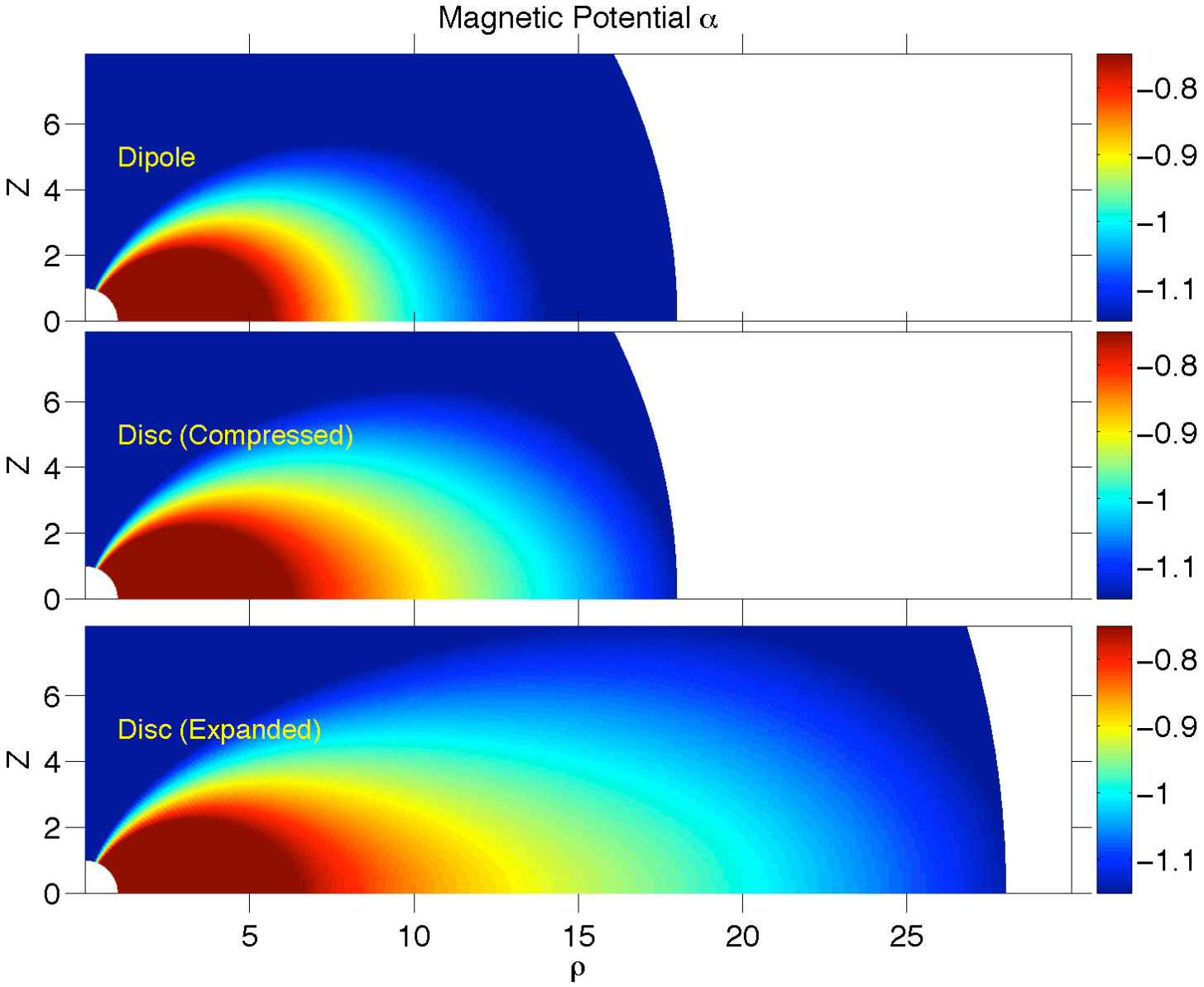

Solutions for the logarithm of magnetic potential α (whose contours are coincident with magnetic field lines) as a function of cylindrical radial distance ρ and vertical distance Z (Z=0 is the equator). Three configurations are shown: Vacuum dipole (top panel); a compressed magnetosphere, Saturn (middle); an expanded magnetosphere, Saturn (bottom). Higher field strengths for the compressed magnetosphere allow curvature forces of similar magnitude to the expanded configuration, but with larger radii of curvature for field lines. Thus for very compressed magnetosphere the radial, disc-like field can vanish [3].

Figure 2: Azimuthal Current Model

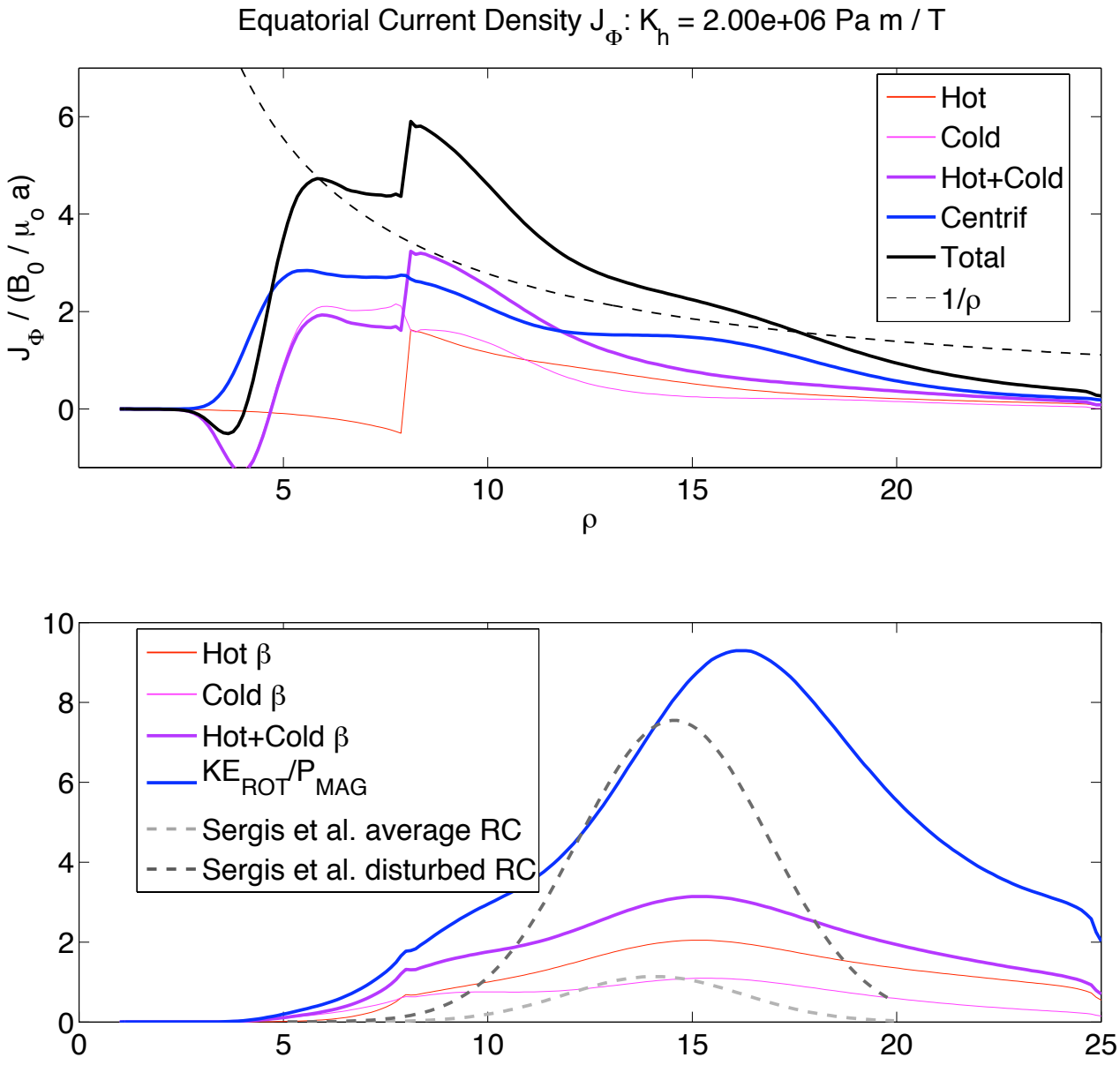

Equatorial radial profiles of normalised current density $\boldsymbol{J}_\phi$ (top panel) and plasma beta (lower panel) for a kronian magnetodisc model with magnetopause radius $R_{MP} = 25\,R_S$ (an average configuration according to [1]).

Figure 2 contd:

Top Panel: Current profiles are colour-coded according to which force is balanced by their contribution to the total $\boldsymbol{J} \times \boldsymbol{B}$ force (hot / cold plasma pressure gradient, centrifugal force). Note that $\boldsymbol{J}_\phi$ falls off more rapidly in the outer magnetosphere than $1/\rho$, the usual function used in the annular disc models of [6]. The negative regions of current balance gradients in plasma pressure which increases with ρ. For $\rho > 12\,\mathrm{R_S}$ the inertial current associated with centrifugal force is the dominant term, although this is also dependent on the hot plasma pressure distribution which may be highly variable.

Lower Panel: Solid lines are profiles of equatorial plasma beta (ratio of plasma pressure / energy density to magnetic pressure), and are colour-coded according to the plasma energy source (hot pressure, cold pressure, rotational kinetic energy of cold plasma). Observations of hot plasma beta by [9] are shown for comparison with our model parameterisation of this quantity, which lies closer to their 'average ring current' profile. The ratio of rotational kinetic energy to plasma pressure reaches its maximum value at the same location as the peak ratio of inertial current (associated with centrifugal force) to curvature / gradient drift current (associated with plasma pressure).

Figure 3: Models vs. Data, Cassini Rev 03

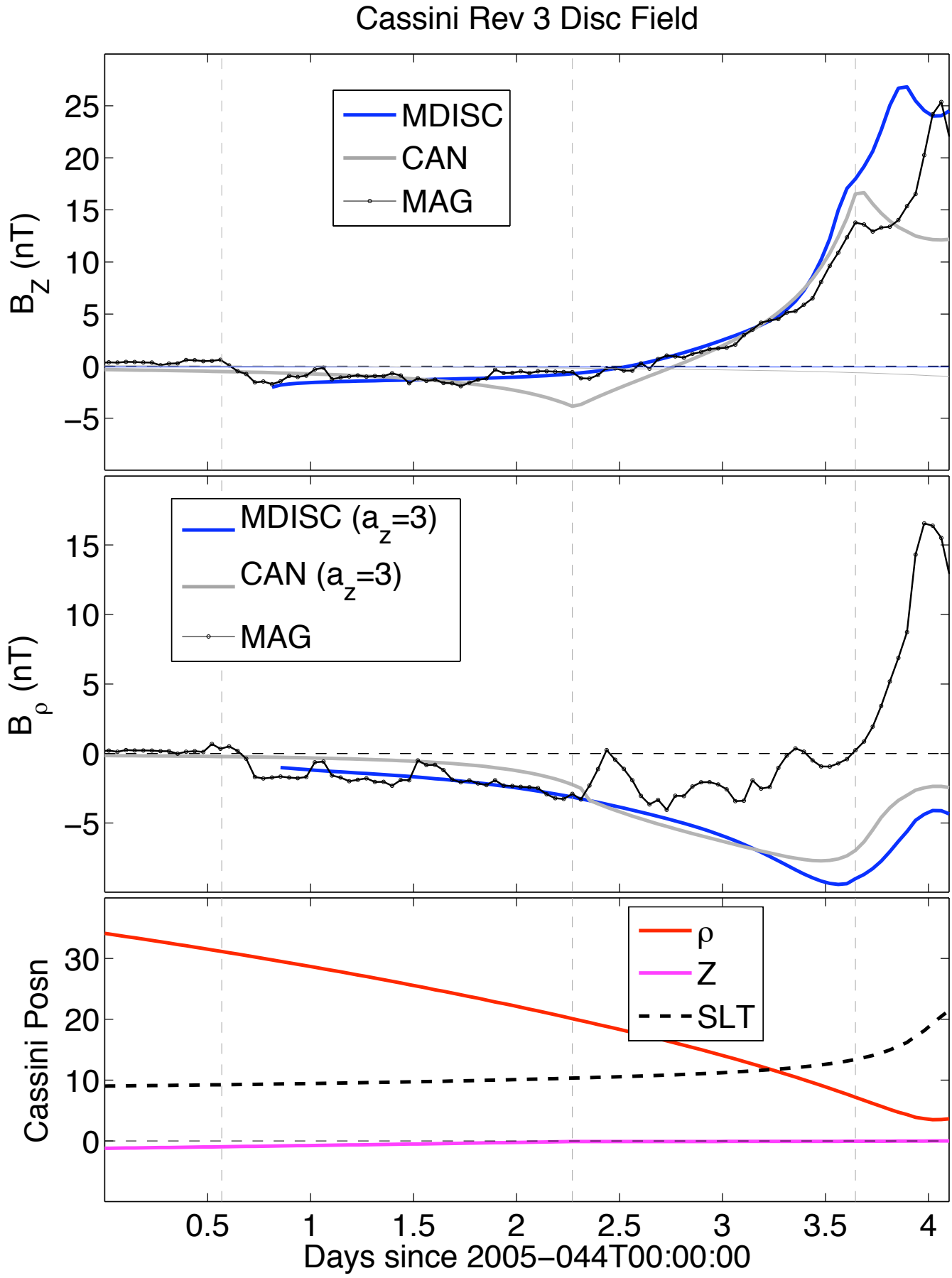

Figure 3 contd:

The top two panels show comparison between modified Cassini magnetometer data from the Rev 3 orbit ('MAG') and models which employ the [6] ('CAN') and Caudalian ('MDISC') discs, with parameters as follows:

- CAN disc parameters were taken from [4], who fit a model to the field observations over many equatorial orbits; the parameters represent a scale current per unit radial length I_o, inner disc radius a, outer disc radius b and disc half-width D, and are $[\mu_o I_o = 53.3\,\mathrm{nT}, a = 7\,\mathrm{R_S}, b = 20\,\mathrm{R_S}, D = 2.5\,\mathrm{R_S}]$.
- The Caudalian disc has two free parameters. These are: (i) magnetopause radius $\mathrm{R_{MP}}$, chosen here to be $30\,\mathrm{R_S}$, according to the position of the last inbound magnetopause crossing and the shape model by [2]; and (ii) hot plasma index K_h (see 'Model Inputs') here set to a value $2 \times 10^6\,\mathrm{Pa\ m\ T^{-1}}$ in order to reproduce average conditions at Saturn (Figure 2).

Thin coloured curves in the top panel represent small contributions from magnetopause and tail currents. Vertical (B_Z) and radial (B_ρ) field components are shown as a function of time. The data are hourly averages and have had the internal field model described by [7] subtracted. The middle panel uses a magnetic equator for the models which is displaced by $3\,\mathrm{R_S}$ north of the planet's rotational equator (without this displacement, the models' predicted values for B_ρ would be identically zero for this equatorial orbit). The bottom panel shows spacecraft position as a function of time (cylindrical radial (ρ) and vertical (Z) distance, Saturn local time (SLT)). Vertical dashed lines indicate, from left to right, the last inbound magnetopause crossing, the inner edge of the CAN model disc ($7\,\mathrm{R_S}$) and the outer edge of this model ($20\,\mathrm{R_S}$).

Figure 4: Models vs. Data, Cassini Rev 40

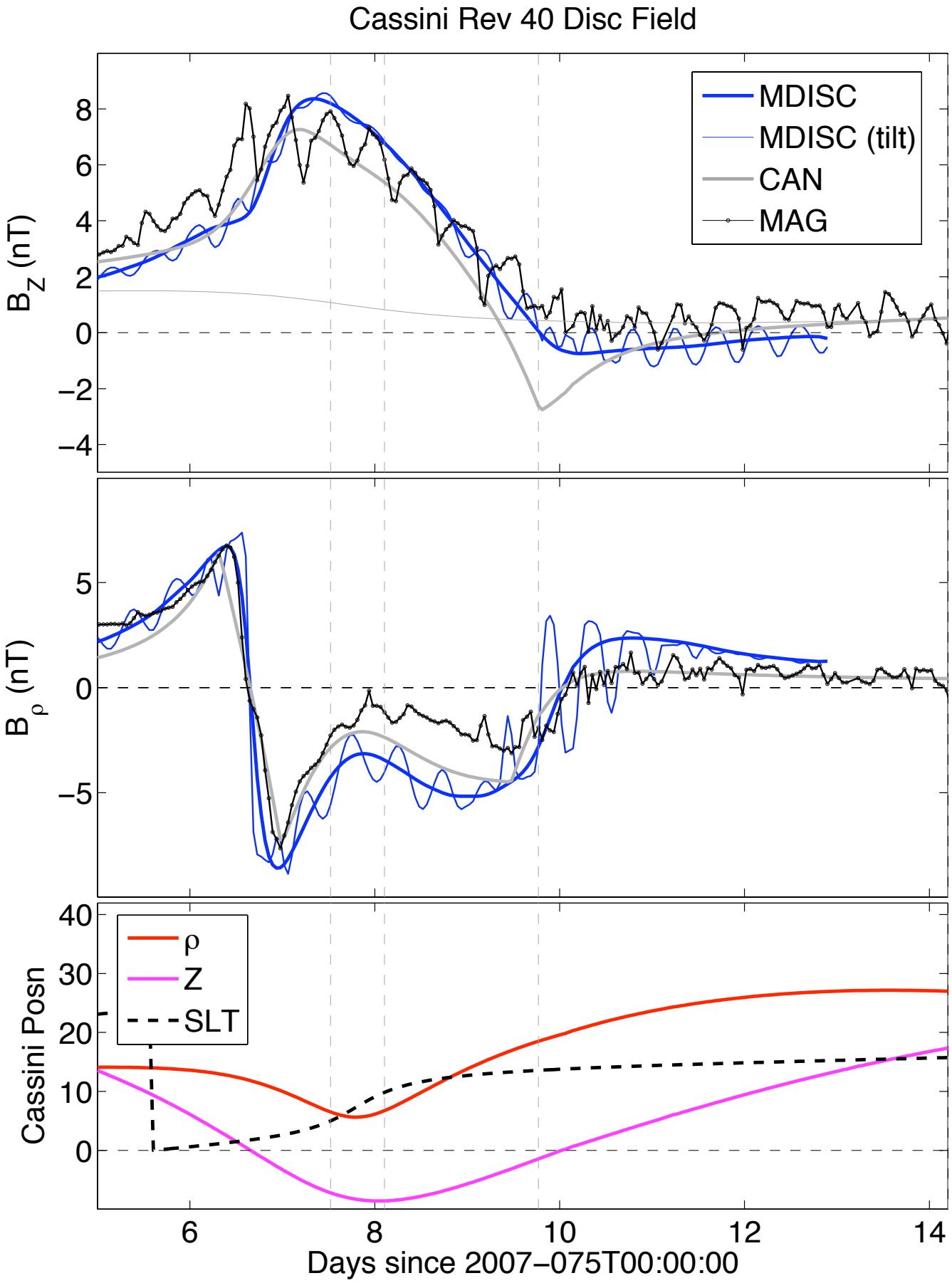

Figure 4 contd:

The top two panels show comparison between modified Cassini magnetometer data from the Rev 40 orbit ('MAG') and models which employ the Connerney ('CAN') and Caudalian ('MDISC') discs (see Figure 3 for details). The Caudalian disc from Figure 3 was also used here, while a CAN disc with the following parameters was used: [$\mu_o I_o = 40\,\mathrm{nT}$, $a = 6.6\,\mathrm{R_S}$, $b = 18.6\,\mathrm{R_S}$, $D = 3.2\,\mathrm{R_S}$].

Vertical (B_Z) and radial (B_ρ) field components are shown as a function of time. The data are hourly averages and have had the internal field model described by [7] subtracted. We also show predictions for a rotating Caudalian disc whose axis is tilted at 10° to that of the planet's rotation axis ('MDISC (tilt)'). The bottom panel shows the spacecraft position as a function of time (cylindrical radial (ρ) and vertical (Z) distance, Saturn local time (SLT)). The vertical dashed lines indicate the positions of the inner ($6.6\,\mathrm{R_S}$) and outer ($18.6\,\mathrm{R_S}$) radii of the CAN disc, whose parameters have been chosen to best fit the B_ρ data. The time axis is truncated on the right at the first outbound magnetopause crossing.

The Caudalian disc has no discontinuous edges nor boundaries, and so shows smoother predicted field profiles than the CAN model, especially near the edges and boundaries of the latter. While a tilted disc model qualitatively reproduces the outer magnetospheric fluctuations in the B_z field, it is clearly inadequate at maintaining these fluctuations in the core region $< 15\,\mathrm{R_S}$. Such a model also cannot explain the drifting period of this fluctuation, also known as the camshaft signal (e.g. [10]).

Figure 5: Beyond the Planar Disc

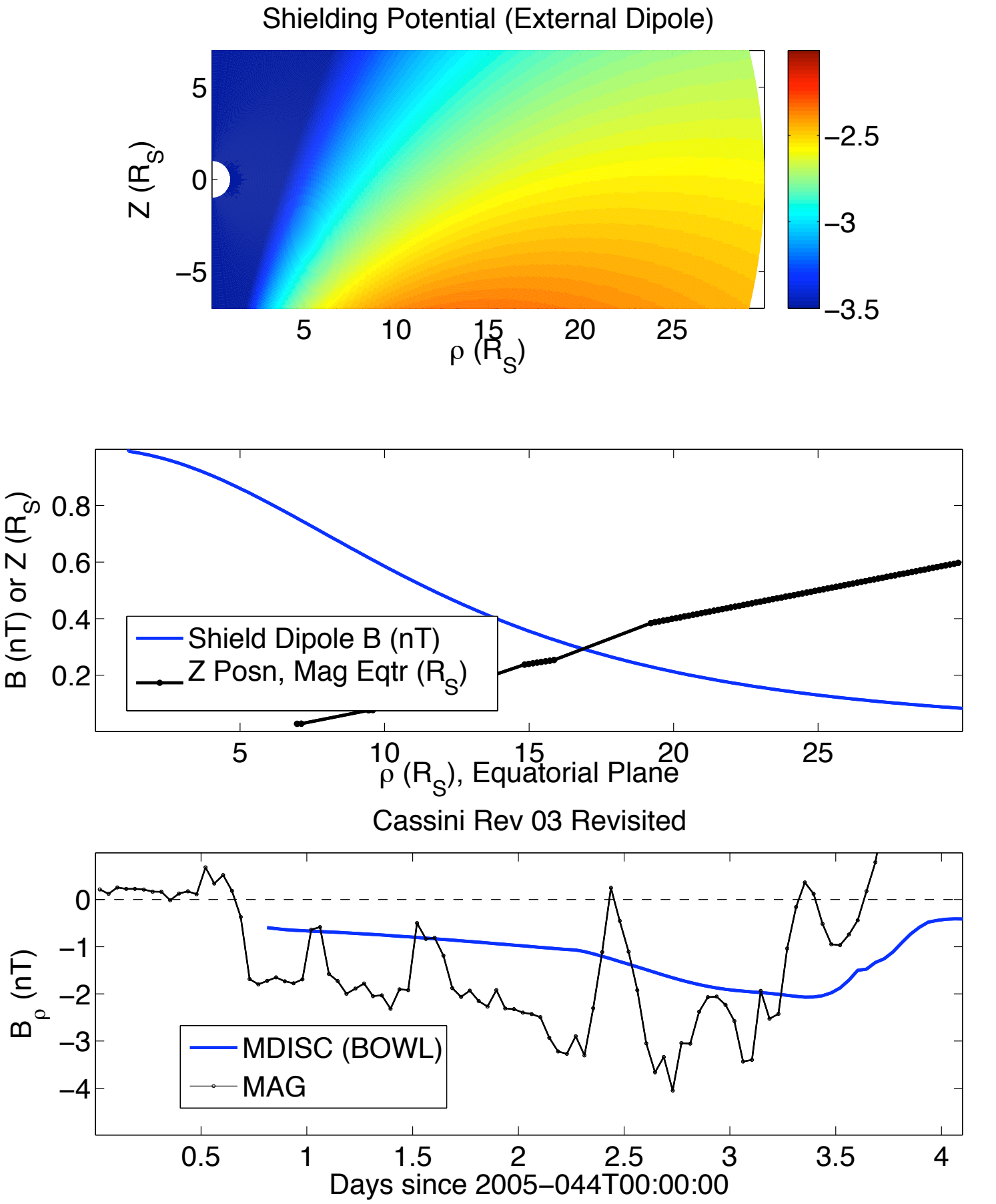

Figure 5 contd:

Top Panel: Logarithm of Euler potential (contours are also field lines) for an external dipole displaced $\sim 17\,\mathrm{R_S}$ south of the planet. We use this field source as an alternative to the usual uniform B_Z due to magnetopause currents in our model. The external dipole represents a magnetopause 'shielding field' with north-south asymmetry which alters the structure of the magnetodisc: the magnetic equator changes from being planar to being slightly 'bowl-shaped'.
Middle Panel: The field strength due to the chosen external dipole, sampled along the rotational equator ($Z = 0$). Also shown is the position of the magnetic equator above the rotational equator in the bowl-shaped disc model (simply defined here as the locus of $B_r = 0$).
Bottom Panel: Here we revisit Cassini Rev 03 (see Figure 3) and compare the B_ρ field of the bowl-shaped disc with the magnetometer data. The model produces a field profile of the same order of magnitude as the data, with B_ρ returning to near-zero closer to the planet where the magnetic and rotational equators are more closely-aligned. Future studies will consider the effect of two factors on the model B_ρ profile: (i) The magnetic moment of the external dipole, which sets the mean value of the predicted field; (ii) The offset of the external dipole relative to the planet, which determines the change in orientation of the shielding field with distance (see Top Panel).

References

[1] N. Achilleos, C. S. Arridge, et al. Large-scale dynamics of Saturn's magnetopause. *J. Geophys. Res.*, 113:A11209, 2008.

[2] C. S. Arridge, N. Achilleos, et al. Modeling the size and shape of Saturn's magnetopause with variable dynamic pressure. *J. Geophys. Res.*, 111:A11227, 2006.

[3] C. S. Arridge, C. T. Russell, K. K. Khurana, N. Achilleos, S. W. H. Cowley, M. K. Dougherty, D. J. Southwood, and E. J. Bunce. Saturn's magnetodisc current sheet. *J. Geophys. Res.*, 113(A12):4214–+, April 2008.

[4] E. J. Bunce, S. W. H. Cowley, I. I. Alexeev, C. S. Arridge, M. K. Dougherty, J. D. Nichols, and C. T. Russell. Cassini observations of the variation of Saturn's ring current parameters with system size. *J. Geophys. Res.*, 112(A11):10202–+, October 2007.

[5] G. Caudal. A self-consistent model of Jupiter's magnetodisc including the effects of centrifugal force and pressure. *J. Geophys. Res.*, 91:4201–4221, April 1986.

[6] J. E. P. Connerney, M. H. Acuna, and N. F. Ness. Saturn's ring current and inner magnetosphere. *Nature*, 292:724–726, August 1981.

[7] M. K. Dougherty, N. Achilleos, N. Andre, C. S. Arridge, A. Balogh, C. Bertucci, M. E. Burton, S. W. H. Cowley, G. Erdos, G. Giampieri, K.-H. Glassmeier, K. K. Khurana, J. Leisner, F. M. Neubauer, C. T. Russell, E. J. Smith, D. J. Southwood, and B. T. Tsurutani. Cassini Magnetometer Observations During Saturn Orbit Insertion. *Science*, 307:1266–1270, February 2005.

[8] M. Kane, D. G. Mitchell, J. F. Carbary, S. M. Krimigis, and F. J. Crary. Plasma convection in Saturn's outer magnetosphere determined from ions detected by the Cassini INCA experiment. *Geophys. Res. Lett.*, 35:4102–+, February 2008.

[9] N. Sergis, S. M. Krimigis, et al. Ring current at Saturn... *Geophys. Res. Lett.*, 34:L09102, 2007.

[10] D. J. Southwood and M. G. Kivelson. Saturnian magnetospheric dynamics: Elucidation of a camshaft model. *J. Geophys. Res.*, 112:A12222, 2007.

[11] R. J. Wilson, R. L. Tokar, M. G. Henderson, T. W. Hill, M. F. Thomsen, and D. H. Pontius. Cassini plasma spectrometer thermal ion measurements in Saturn's inner magnetosphere. *J. Geophys. Res.*, 113:A12218, December 2008.